

Revisiting the Higgs Mass and Dark Matter in the CMSSM

John Ellis¹ and Keith A. Olive²

¹*Theoretical Particle Physics and Cosmology Group, Department of Physics,
King's College London, London WC2R 2LS, United Kingdom;
Theory Division, CERN, CH-1211 Geneva 23, Switzerland*

²*William I. Fine Theoretical Physics Institute, School of Physics and Astronomy,
University of Minnesota, Minneapolis, MN 55455, USA*

Abstract

Taking into account the available accelerator and astrophysical constraints, the mass of the lightest neutral Higgs boson h in the minimal supersymmetric extension of the Standard Model with universal soft supersymmetry-breaking masses (CMSSM) has been estimated to lie between 114 and ~ 130 GeV. Recent data from ATLAS and CMS hint that $m_h \sim 125$ GeV, though $m_h \sim 119$ GeV may still be a possibility. Here we study the consequences for the parameters of the CMSSM and direct dark matter detection if the Higgs hint is confirmed, focusing on the strips in the $(m_{1/2}, m_0)$ planes for different $\tan\beta$ and A_0 where the relic density of the lightest neutralino χ falls within the range of the cosmological cold dark matter density allowed by WMAP and other experiments. We find that if $m_h \sim 125$ GeV focus-point strips would be disfavoured, as would the low- $\tan\beta$ $\tilde{\tau} - \chi$ and $\tilde{t}_1 - \chi$ coannihilation strips, whereas the $\tilde{\tau} - \chi$ coannihilation strip at large $\tan\beta$ and $A_0 > 0$ would be favoured, together with its extension to a funnel where rapid annihilation via direct-channel H/A poles dominates. On the other hand, if $m_h \sim 119$ GeV more options would be open. We give parametrizations of WMAP strips with large $\tan\beta$ and fixed $A_0/m_0 > 0$ that include portions compatible with $m_h = 125$ GeV, and present predictions for spin-independent elastic dark matter scattering along these strips. These are generally low for models compatible with $m_h = 125$ GeV, whereas the XENON100 experiment already excludes some portions of strips where m_h is smaller.

February 2012

1 Introduction

Since supersymmetry relates the Higgs self-coupling to electroweak gauge couplings, it is a characteristic prediction of the minimal supersymmetric extension of the Standard Model (MSSM) that the lightest neutral Higgs boson h should be relatively light. This prediction is in agreement with the indirect indications from precision electroweak data, which favour $m_h \sim 100$ GeV [1]. Indeed, at the tree level m_h would be $< m_Z$, but radiative corrections due principally to the top squarks may increase m_h to ~ 130 GeV within the MSSM [2]. The latest LHC searches for a Standard Model-like Higgs boson exclude the mass range $m_h \in (127, 600)$ GeV at the 95% CL, but leave open the range $m_h \in (115.5, 127)$ GeV, which is consistent with the MSSM prediction [3]. Moreover, within this range ATLAS sees an excess of events with $m_h \sim 126$ GeV [4], and CMS sees a broader excess extending over the range $m_h \in (119, 125)$ GeV [5]. The observations of these excesses are more significant within the MSSM than in the general Standard Model context, since the look-elsewhere effect is diminished for the restricted Higgs mass range predicted previously within the MSSM.

Identifying the lightest neutralino χ as the dominant component of dark matter provides an important constraint on the MSSM parameter space [6] that can be quantified within any specific framework for supersymmetry breaking. Here we assume the CMSSM [7–13], in which the soft supersymmetry-breaking parameters $m_{1/2}, m_0$ and A_0 are constrained to be universal at the GUT scale. In the CMSSM, there are narrow strips of parameter space where the relic χ density falls within the narrow range indicated by WMAP and other astrophysical and cosmological measurements [14], which we take to be $\Omega_\chi h^2 = 0.112 \pm 0.12$ corresponding to a conservative $2 - \sigma$ range. These strips include one where coannihilation between χ , the lighter stau $\tilde{\tau}_1$ and other sleptons brings the cold dark matter density into the WMAP range [15], which at large $\tan\beta$ extends into a funnel where annihilations via direct-channel H/A resonances are dominant [7,9], and a focus-point strip at large m_0 where annihilation is enhanced by a significant Higgsino component in the composition of χ [16]. When A_0 is large, there may also be a strip where χ coannihilation with the lighter stop \tilde{t}_1 is important [17].

These strips are useful for benchmarking searches for supersymmetry at colliders [18] and searches for astrophysical dark matter [19], e.g., via direct searches for elastic scattering [20] or via searches for energetic neutrinos produced by dark matter annihilations in the core of the Sun or Earth [21], or via searches for energetic photons from dark matter annihilations near the centre of the Galaxy [22] or elsewhere. It is therefore important that the benchmark strips should be updated to take the latest accelerator and other constraints into account [23].

This is the main purpose of this paper, with particular focus on highlighting (portions of) strips that are compatible with a hypothetical measurement of m_h , and their implications for dark matter detection.

It is a general feature of relic density calculations that they yield an upper limit on the magnitudes of $m_{1/2}$ and m_0 , and hence on m_h . This connection was explored in [24], with the result that an upper bound $m_h \sim 127$ GeV was found within the CMSSM, after the experimental, phenomenological, astrophysical and cosmological constraints then available were taken into account. This result was confirmed in a recent global frequentist analysis of constraints on the CMSSM [13, 25–27]. It is encouraging that the excesses found by ATLAS and CMS fall within the range allowed by these analyses.

Within a specific framework such as the CMSSM, a measurement of m_h would impose a complementary constraint on the strips of parameter space allowed by the dark matter density, although with some uncertainty due to the error $\sim \pm 1.5$ GeV associated with the theoretical calculation of m_h for any given value of the CMSSM parameters [28]. The impact of this constraint on the CMSSM was explored recently [27, 29], for the values $m_h \sim 125$ and 119 GeV suggested by the recent ATLAS and CMS results. It was shown, in particular, that relatively large values of $m_{1/2}, m_0, A_0$ and $\tan \beta$ would be favoured if $m_h \sim 125$ GeV.

In this paper we explore in more detail the potential implications of an LHC measurement of $m_h \sim 125$ or 119 GeV for the WMAP-compatible strips of the CMSSM, concentrating on the case $\mu > 0$. We find that a measurement of $m_h \sim 125$ GeV would favour the $\tilde{\tau}_1 - \chi$ coannihilation strip and its extension to the rapid H/A annihilation funnel at large $\tan \beta$ with $A_0 > 0$, and disfavour the low- $\tan \beta$ $\tilde{\tau}_1 - \chi$ coannihilation strip, as well as the $\tilde{t}_1 - \chi$ coannihilation and focus-point strips (except if $m_0 > 5000$ GeV). On the other hand, a measurement of $m_h \sim 119$ GeV would keep these options open. We also discuss the interplay within the CMSSM between m_h and the elastic dark matter scattering cross section. We find that, whereas some low- m_h models are already excluded by the XENON100 experiment [30], models with $m_h \sim 125$ GeV typically predict cross sections well below the present experimental sensitivity.

2 Summary of Results from Scans of the CMSSM Parameter Space

As mentioned in the Introduction, in 2005 a scan of the CMSSM parameter space was made over the ranges $100 \text{ GeV} < m_{1/2} < 2 \text{ TeV}$, $m_0 < 2 \text{ TeV}$, $|A_0/m_{1/2}| < 3$, $2 < \tan \beta < 58$ and $\mu > 0$, mostly with $m_t = 174.3$ GeV though other values of m_t were also considered in

less detail. The principal result of this scan was a histogram of m_h shown in Fig. 1 of [24], which displayed a range extending up to ~ 127 GeV. This is reproduced in the upper left panel of Fig. 1, with vertical green bands added to indicate the ranges $m_h = 119 \pm 1.5$ GeV and 125 ± 1.5 GeV hinted by LHC data [4, 5]. It is encouraging that the range found in [24] includes the value $m_h \sim 125$ GeV currently preferred by ATLAS and CMS. However, it is equally clear that this value is far from the mode of the histogram. The lower left panel of Fig. 1 displays the (relatively few) points compatible with $m_h = 125$ GeV as calculated using `FeynHiggs` [28] within the theoretical error of ± 1.5 GeV, highlighting (in red) the (very few) points favoured by $g_\mu - 2$ [33] at the $2 - \sigma$ level. We see that most of the points compatible with $m_h = 125$ GeV have $m_{1/2}$ and m_0 both > 1 TeV, whereas the $g_\mu - 2$ -compatible points are concentrated at small values of $m_{1/2}$ and m_0 . We do not reproduce here the histogram of values of $\tan \beta$ shown in Fig. 2 of [24], but recall that it was concentrated at $\tan \beta > 50$, with a tail extending down to $\tan \beta \sim 10$. The upper right panel of Fig. 1 shows that the CMSSM points compatible with $m_h \sim 125$ GeV are concentrated at large values of $A_0 > 0$.

On the other hand, it is clear from the upper left panel of Fig. 1 that the 2005 scan found more points with $m_h \sim 119$ GeV (though this was also not a mode of the m_h histogram!) and we see from the lower right panel of Fig 1 that many of these points had $m_{1/2}$ and/or $m_0 < 1$ TeV. As seen in the upper right panel of Fig. 1, points with $m_h \sim 119$ GeV exhibit no preference for either sign of A_0 .

Recently, as members of the `MasterCode` collaboration, we have participated in a frequentist analysis of the relative likelihoods of different points in the CMSSM parameter space incorporating the constraints from LHC missing-energy searches [31] on supersymmetric particles with $\sim 1/\text{fb}$ of data [26]. This analysis favoured $m_h \sim 119$ GeV, with a likelihood price $\Delta\chi^2 \sim 2$ for a hypothetical measurement $m_h \sim 125$ GeV. As shown in [27], such a value of m_h would indicate within the CMSSM a preference for relatively large values of $m_{1/2}, m_0$ and $\tan \beta$, confirming the results of [24]. However, we also note that smaller values of $\tan \beta \sim 10$ are still allowed at the 68% CL even if $m_h \sim 125$ GeV, in association with $m_{1/2} \sim 700$ GeV. The analysis of this paper complements that of [27], by providing more insight into the interplay of the principal constraints and the resulting predictions for direct dark matter detection.

3 Dark Matter Strips

As was reviewed in the Introduction, the requirement that the relic neutralino density falls within the range allowed by WMAP and other observations implies that, the allowed values

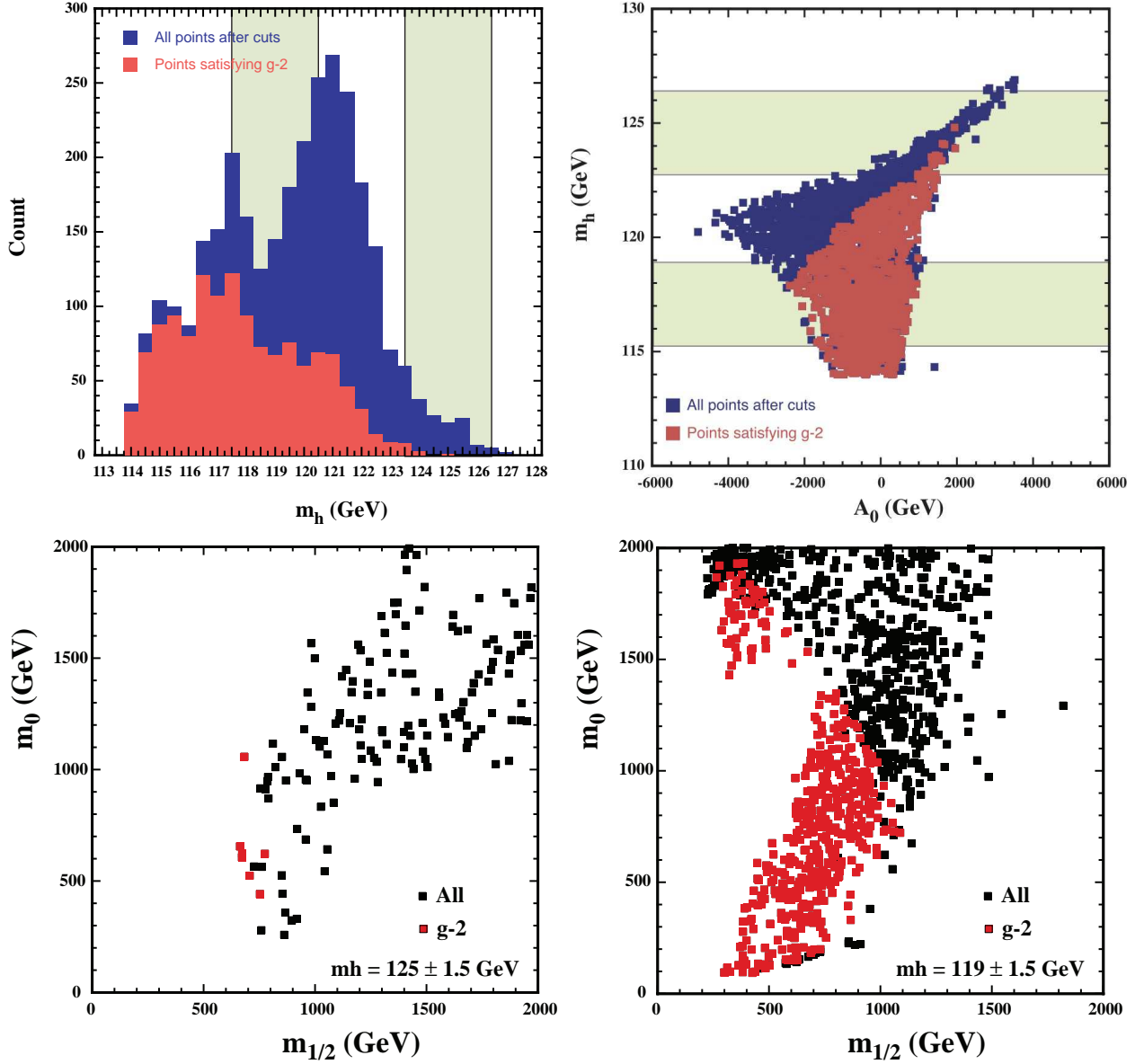


Figure 1: *Upper panels: Histogram of values of m_h found in a pre-LHC scan of the CMSSM parameter space [24] (left), and displaying the corresponding values of A_0 (right). In both panels we have added green bands corresponding to the ranges 119 ± 1.5 GeV and 125 ± 1.5 GeV hinted by the LHC [4, 5]. Lower panels: The distributions of the points from [24] in the $(m_{1/2}, m_0)$ plane of the CMSSM for which FeynHiggs yields $m_h = 125 \pm 1.5$ GeV (left) and 119 ± 1.5 GeV (right). These results were obtained assuming $m_t = 174.3$ GeV. Points favoured by the $g_\mu - 2$ constraint are highlighted in red in all four panels.*

of $m_{1/2}$ and m_0 lie along narrow strips in generic $(m_{1/2}, m_0)$ planes for fixed values of A_0 and $\tan\beta$ [11]. Along these strips, the dominant mechanism fixing the relic density may be coannihilation with some near-degenerate sparticle species, such as the $\tilde{\tau}_1$ or \tilde{t}_1 , or $\chi - \chi$ annihilations facilitated by direct-channel heavy Higgs H/A poles (in rapid-annihilation funnels) or by enhanced Higgsino components (along focus-point strips). As was also mentioned in the Introduction, points along these WMAP-compatible strips are often used as benchmarks [18] for dark matter searches [19], e.g., via scattering [20] or annihilations into neutrinos [21] or photons [22]. These benchmark strips require updating in light of the strengthening LHC constraints on supersymmetry [23] and the hypothetical Higgs mass measurement [4, 5].

Fig. 2 displays the latest incarnations of the $(m_{1/2}, m_0)$ planes for $\mu > 0$, $A_0 = 0$ and $\tan\beta = 10$ (left) and 55 (right) ¹. Here and in subsequent figures, the regions forbidden because the LSP is charged are shaded brown, the regions where there is no consistent electroweak vacuum are shaded (darker) pink, the regions excluded by $b \rightarrow s\gamma$ [32] are shaded green, the regions favoured by $g_\mu - 2$ [33] at the $\pm 2 - \sigma$ level are shaded (paler) pink, and the WMAP-compatible dark matter strips are shaded dark blue. The black dashed line is the $m_{\chi_1^\pm} = 104$ GeV contour, the solid purple lines outline the 95% CL constraints on $(m_{1/2}, m_0)$ in the CMSSM imposed by missing-energy searches at the LHC [31], and contours of m_h as calculated using `FeynHiggs` [28] are shown as red dash-dotted lines. Here, and in all subsequent analyses, a top quark mass of 173.2 GeV was used [34]. We see that $m_h = 119 \pm 1.5$ GeV is compatible with the dark matter constraint only for $m_{1/2} > 640$ GeV if $\tan\beta = 10$, and for $m_{1/2} > 560$ GeV if $\tan\beta = 55$. These regions are in the upper portions of the $\tilde{\tau}_1 - \chi$ coannihilation strips, which extend to $m_{1/2} \sim 900$ GeV. The contours $m_h = 125 \pm 1.5$ GeV are nowhere to be seen as, e.g., nominal `FeynHiggs` values of m_h do not exceed ~ 120 GeV for $m_0 < 3000$ GeV along the focus-point strip for $\tan\beta = 55$ and $A_0 = 0$.

Guided by the upper right panel of Fig. 1, we now consider $(m_{1/2}, m_0)$ planes for $A_0 > 0$. Initially, we consider in Fig. 3 examples with fixed $A_0 = 3$ TeV (except for the lower right panel, where $A_0 = 2$ TeV) and $\tan\beta = 10$ (upper left panel), 40 (upper right panel), and 55 (lower panels) ². When $\tan\beta = 10$ and 40, we see brown shaded regions at low $m_{1/2}$ and m_0 where the LSP is the lighter stop, \tilde{t}_1 , which expand with increasing A_0 . There are

¹As already mentioned, we focus here on $\mu > 0$. This assumption was motivated in the past by indications from $g_\mu - 2$ and the desire to avoid strong constraints from $b \rightarrow s\gamma$ [32], but should perhaps be reviewed now in light of the growing tension between LHC missing-energy constraints [31] and $g_\mu - 2$ [33].

²The true WMAP strips corresponding to $\Omega_\chi h^2 = 0.112 \pm 0.012$ [14] at the $2 - \sigma$ level are often invisibly narrow. Accordingly, in these and most subsequent figure panels, the WMAP strips have been made more visible by colouring regions where $0.05 < \Omega_\chi h^2 < 0.15$.

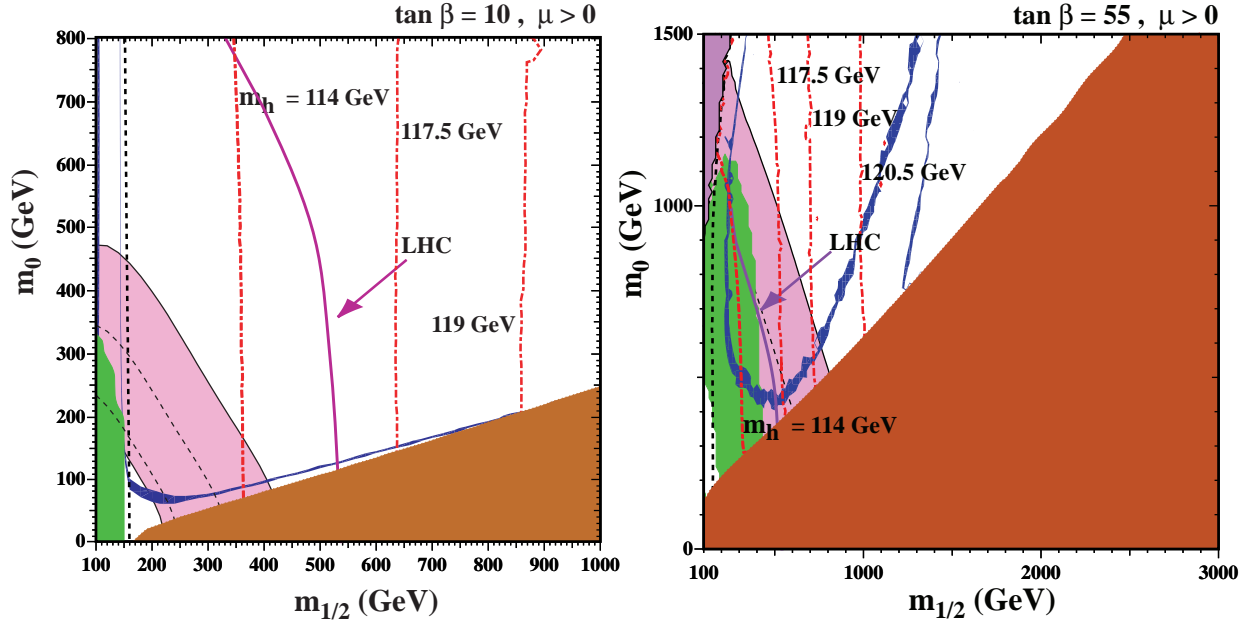


Figure 2: The $(m_{1/2}, m_0)$ planes for $\mu > 0$, $A_0 = 0$ and $\tan \beta = 10$ (left) and 55 (right), as calculated for $m_t = 173.2$ GeV using the latest version of the SSARD code [35]. The WMAP strips where $\Omega_\chi h^2 = 0.112 \pm 0.012$ are shaded dark blue: note the narrow coannihilation strip in the left panel and the coannihilation strip, rapid-annihilation funnel and focus-point strip in the right panel. The other shadings and colours of the contours are described in the text.

$\tilde{t}_1 - \chi$ coannihilation strips running close to their outer boundaries, portions of which are compatible with $m_h \sim 119$ GeV when $\tan \beta = 10$. However, this coannihilation region is excluded by $b \rightarrow s\gamma$ for $\tan \beta = 40$. In the $\tan \beta = 10$ case there is also a portion of the $\tilde{\tau}_1 - \chi$ coannihilation strip at $m_{1/2} \sim 700$ GeV that is compatible with $m_h \sim 119$ GeV, but no region with $m_h \sim 125$ GeV can be seen. On the other hand, when $\tan \beta = 40$ and $A_0 = 3$ TeV, we see that there is a portion of the $\tilde{\tau}_1 - \chi$ coannihilation strip around $m_{1/2} \sim 800$ GeV that is compatible with $m_h = 125$ GeV. When $\tan \beta = 55$ (lower panels of Fig. 3), the $\tilde{t}_1 - \chi$ coannihilation strips disappear, and the $\tilde{\tau}_1 - \chi$ coannihilation strip morphs into the H/A rapid-annihilation funnel for $m_{1/2} \sim 1500$ GeV³. In both the cases $A_0 = 3000$ GeV (lower left panel) and $A_0 = 2000$ GeV (lower right panel), in the funnel regions there are portions of the WMAP-compatible strips that are compatible with $m_h = 125$ GeV, within the expected FeynHiggs uncertainty of ± 1.5 GeV. These examples confirm that larger values of $\tan \beta \sim 40$ or more and $A_0 > 0$ would be favoured if $m_h = 125$ GeV, as already suggested by the upper right panel of Fig. 1 and the right panel of Fig. 2. Finally, we note that there

³Also visible in these panels between $m_{1/2} \sim 1000$ GeV and ~ 1500 GeV is another WMAP-compatible strip running roughly parallel to the $\tilde{\tau}_1 - \chi$ coannihilation strip, which is due to rapid $\tilde{\tau}_1 - \bar{\tilde{\tau}}_1$ annihilation through direct-channel H/A poles.

is no $g_\mu - 2$ -friendly region in any panel of Fig. 3.

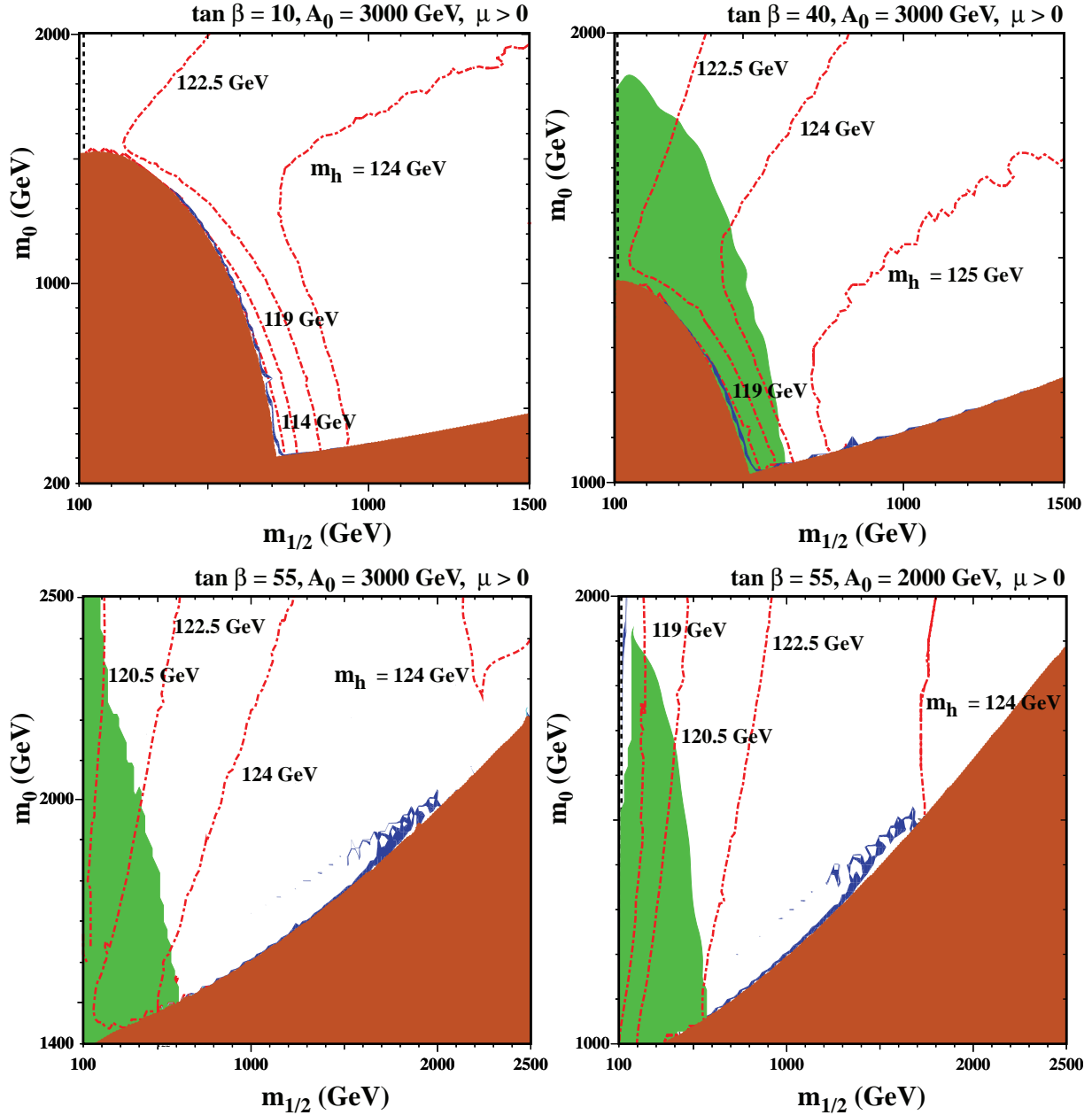


Figure 3: As Fig. 2, with $\tan \beta = 10$ in the upper left panel, $\tan \beta = 40$ in the upper right panel, and $\tan \beta = 55$ in the lower panels. We choose $A_0 = 3000$ GeV, except in the lower right panel where $A_0 = 2000$ GeV.

Simple supergravity models of soft supersymmetry breaking suggest a relation between A_0 and m_0 of the form $A_0 = c.m_0$ for some constant $c \in [-3, 3]$. In this context, the fixed values of A_0 chosen in Fig. 3 might appear quite extreme for small values of m_0 , e.g.,

near the junction of the $\tilde{\tau}_1$ and \tilde{t}_1 coannihilation strips in the upper left panel, where we find $m_h \sim 124$ GeV for $m_0 \sim 350$ GeV. Therefore, we display in Fig. 4 some examples of $(m_{1/2}, m_0)$ planes for fixed ratios $A_0/m_0 = 2$ (upper panels and lower left panel) and 1.5 (lower right panel). The upper left panel is for $\tan \beta = 10$, the upper right for $\tan \beta = 40$, and the lower panels for $\tan \beta = 55$. As $\tan \beta$ increases for fixed $A_0/m_0 = 2$, we see that the contours of m_h move towards smaller values of $(m_{1/2}, m_0)$, whereas the region disallowed by $b \rightarrow s\gamma$ expands to larger $(m_{1/2}, m_0)$. When $\tan \beta = 10$ (upper left panel of Fig. 4), we note that there is a forbidden \tilde{t}_1 LSP region at small $m_{1/2}$ and large m_0 , which disappears for $\tan \beta = 40$, and is replaced for $\tan \beta = 55$ by a region where electroweak symmetry breaking is absent. The focus-point strip adjacent to the boundary of this region is forbidden by $b \rightarrow s\gamma$ out to larger values of m_0 and $m_{1/2}$ than those shown. In the lower right panel, the coannihilation strip extends into a rapid-annihilation funnel compatible with $m_h = 125$ GeV, and we see again a rapid $\tilde{\tau}_1 - \tilde{\bar{\tau}}_1$ annihilation strip.

When $\tan \beta = 10$, there is a portion of the $\tilde{\tau}_1 - \chi$ coannihilation strip with $m_{1/2} \sim 700$ GeV that is compatible with $m_h = 119$ GeV, and also a portion of the \tilde{t}_1 coannihilation strip with $m_0 \sim 1000$ GeV, but no visible region allowed by WMAP is compatible with $m_h = 125$ GeV. When $\tan \beta = 40$, the portion of the $\tilde{\tau}_1 - \chi$ coannihilation strip compatible with $m_h = 119$ GeV moves down to $m_{1/2} \sim 500$ GeV, and is one of the few cases compatible with $g_\mu - 2$, but $m_h = 125$ GeV is still not allowed. When $\tan \beta = 55$ and $A_0 = 2m_0$ there is a substantial stretch of the $\tilde{\tau}_1 - \chi$ coannihilation strip that is compatible with $m_h = 125$ GeV. When $\tan \beta = 55$ and $A_0 = 1.5m_0$ (lower right panel), the values of m_h are generally reduced, but $m_h = 125$ GeV is still possible in the rapid-annihilation funnel extension of the $\tilde{\tau}_1 - \chi$ coannihilation strip at $m_{1/2} \sim 2000$ GeV, and $m_h = 119$ GeV is possible for $m_{1/2} \sim 600$ GeV, in a portion of the $\tilde{\tau}_1 - \chi$ coannihilation strip that is compatible with both $b \rightarrow s\gamma$ and $g_\mu - 2$. In this case, WMAP becomes compatible with $m_h = 125$ GeV along the focus point strip when $m_0 > 5000$ GeV.

We note that when $\tan \beta = 40$ or 55 the region forbidden by $b \rightarrow s\gamma$ is split in two parts at smaller and larger $m_{1/2}$, separated by a strip that is allowed. This occurs because $\text{BR}(b \rightarrow s\gamma)$ is too large at small $m_{1/2}$, falls through the acceptable range as $m_{1/2}$ increases, becoming unacceptably small because of cancellations over a range of $m_{1/2}$, before rising towards the Standard Model value at large $m_{1/2}$. Portions of the $b \rightarrow s\gamma$ -compatible band are compatible with the cold dark matter density and/or $g_\mu - 2$, and there are also small ranges of parameters where $m_h \sim 119$ GeV is possible.

In Fig. 5 we display similar $(m_{1/2}, m_0)$ planes for $\tan \beta = 10$ (left panel) and $\tan \beta = 40$ (right panel), both with larger $A_0/m_0 = 2.5$. In these cases, we see expanded \tilde{t}_1 LSP regions

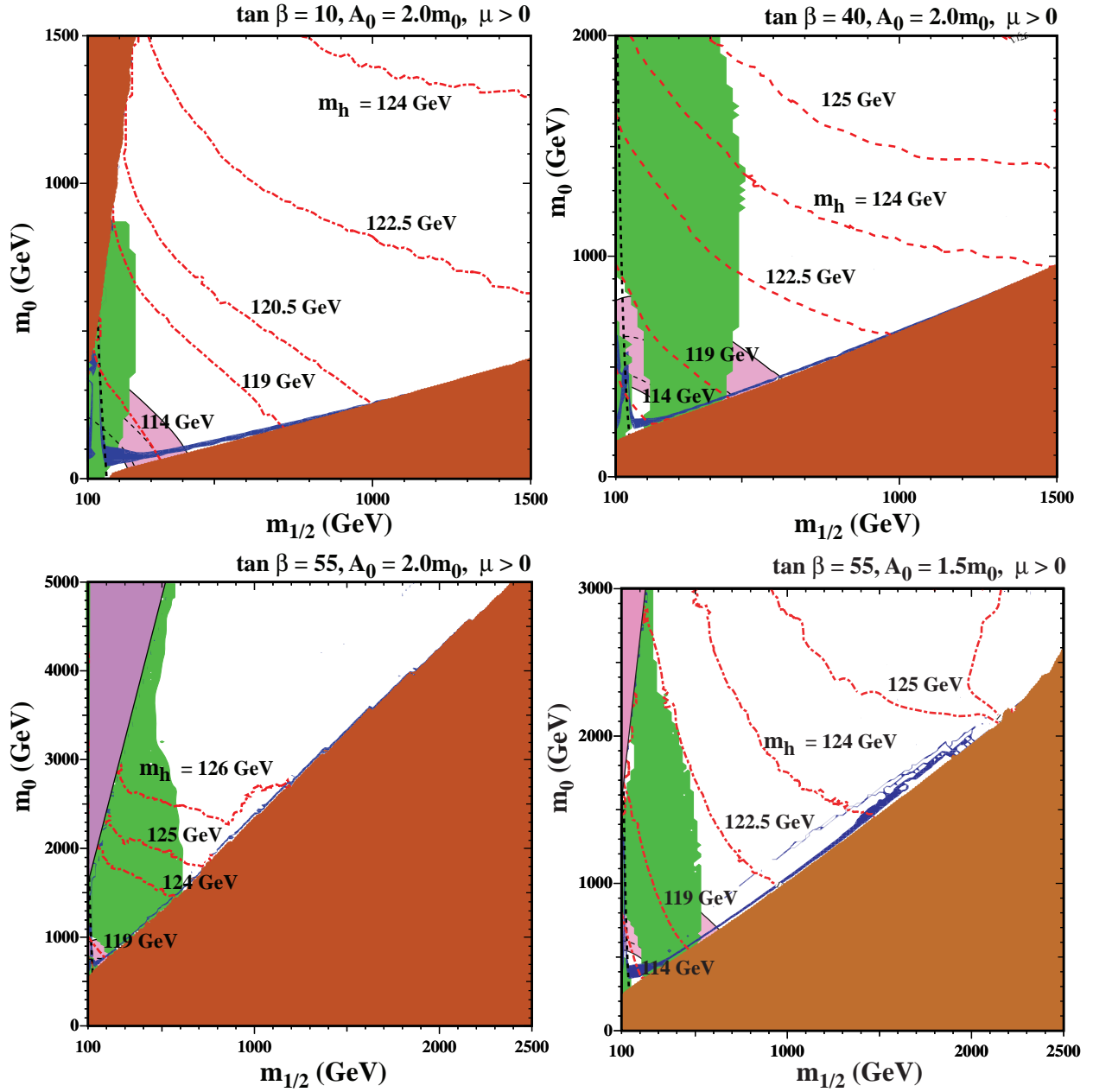


Figure 4: As Fig. 2, with $\tan \beta = 10$ (upper left panel), $\tan \beta = 40$ (upper right panel) and $\tan \beta = 55$ in the lower panels. We choose $A_0 = 2m_0$, except in the lower right panel where $A_0 = 1.5m_0$.

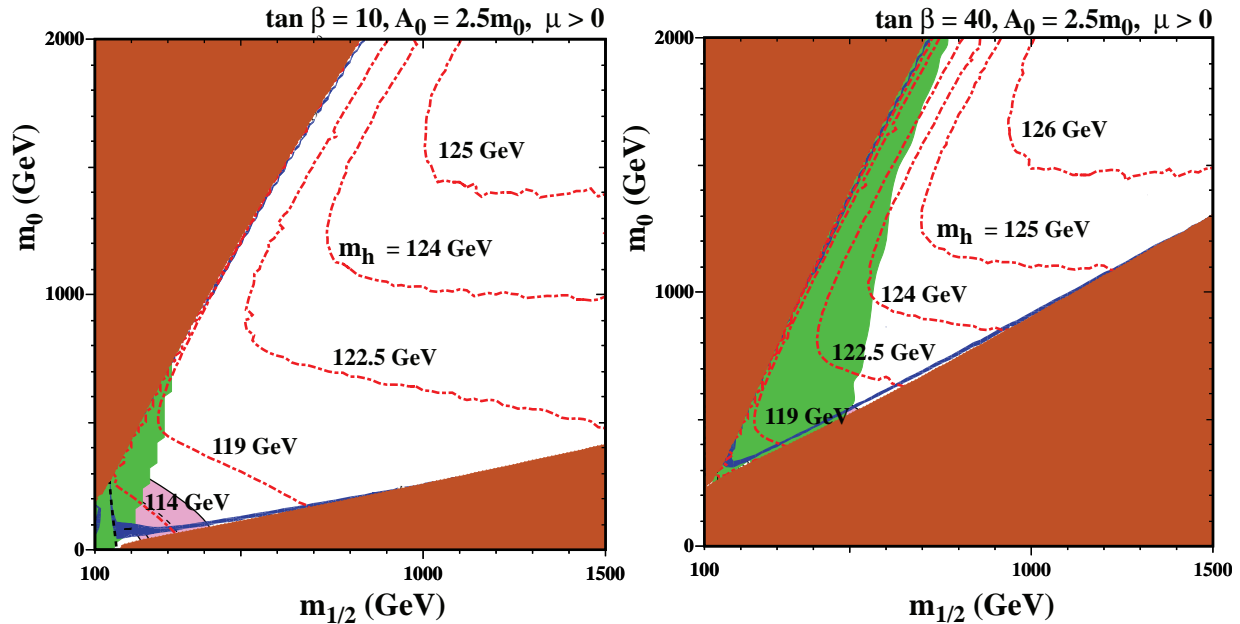


Figure 5: As Fig. 2, with $\tan\beta = 10$, (left panel) and $\tan\beta = 40$ (right panel), for $A_0 = 2.5m_0$.

at large m_0 . In the $\tan\beta = 10$ case, $m_h = 119$ GeV is possible in portions of both the $\tilde{\tau}_1 - \chi$ and $\tilde{t}_1 - \chi$ coannihilation strips. In the $\tan\beta = 40$ case, $m_h = 125$ GeV is possible at large $m_{1/2}$ along the $\tilde{\tau}_1 - \chi$ coannihilation strip, but $b \rightarrow s\gamma$ forbids lower $m_h \sim 119$ GeV, and also excludes the visible part of the $\tilde{t}_1 - \chi$ coannihilation strip. For $\tan\beta = 55$ and $A_0/m_0 = 2.5$, we do not find consistent solutions for generic regions of the $(m_{1/2}, m_0)$ plane.

In order to see from a different perspective the influence of the choice of A_0 , in Fig. 6 we display $(m_{1/2}, A_0)$ planes for $\tan\beta = 10$ (top panels), $\tan\beta = 40$ (middle panels), $\tan\beta = 55$ (bottom panels), and low values of $m_0 = 250, 1000, 1000$ GeV (left panels) compared with the large values $m_0 = 3000, 3000, 2000$ GeV (right panels). In the top left panel for $\tan\beta = 10$ we see a large $\tilde{\tau}_1$ LSP region at large $m_{1/2}$ and two \tilde{t}_1 LSP regions at small $m_{1/2}$ and large $|A_0|$. Adjacent to the boundaries of these regions there are coannihilation strips, and inside the χ LSP region there is a region in conflict with $b \rightarrow s\gamma$ and a region favoured by $g_\mu - 2$. We see clearly that m_h increases with increasing A_0 . There is no portion of the allowed region that is compatible with $m_h = 125$ GeV, but there are two WMAP-compatible regions with $m_h \sim 119$ GeV: along the $\tilde{t}_1 - \chi$ coannihilation strip for $A_0 > 0$ and on the $\tilde{\tau}_1 - \chi$ coannihilation strip where $m_{1/2} \sim 1000$ GeV and $A_0 \sim -500$ GeV. As m_0 is increased, the $\tilde{\tau}_1$ LSP region recedes to large $m_{1/2}$ and the \tilde{t}_1 LSP regions recede to larger $|A_0|$. At the same time, the regions excluded by $b \rightarrow s\gamma$ and the $g_\mu - 2$ -compatible region disappear from the visible area of the $(m_{1/2}, A_0)$ plane. Instead, in the top right panel of Fig. 6 for $\tan\beta = 10$

and $m_0 = 3000$ GeV, we see the appearance of a protuberance where there is no consistent electroweak symmetry breaking, which is surrounded by a focus-point strip. Taking into account the theoretical uncertainties, all the displayed portion of this strip is compatible with $m_h \sim 119$ GeV, with $A_0 > 0$ preferred.

Examples with $\tan\beta = 40$ are shown in the middle panels of Fig. 6. For $m_0 = 1000$ GeV (left panel), we again see $\tilde{\tau}_1$ and \tilde{t}_1 regions flanked by coannihilation strips, which have receded from their locations in the top left panel for $\tan\beta = 10$ and $m_0 = 250$ GeV. We also see a $g_\mu - 2$ -compatible region at small $m_{1/2}$, and note that the region forbidden by $b \rightarrow s\gamma$ has expanded as compared with the top left panel. The only WMAP compatible region where $m_h \sim 125$ GeV is at $m_{1/2} \sim 500$ to 1500 GeV with $A_0 > 2000$ GeV, whereas $m_h \sim 119$ GeV is possible only for $A_0 < -3000$ GeV. Turning to the case $\tan\beta = 40$, $m_0 = 3000$ GeV (middle right panel of Fig. 6), we see that the protuberance without electroweak symmetry breaking has expanded. In this case all the surrounding focus-point strip is compatible with $m_h \sim 119$ GeV, but $m_h = 125$ GeV is out of reach.

Turning finally to the bottom panels of Fig. 6 for $\tan\beta = 55$, we see new features, namely rapid-annihilation funnels centred around $m_{1/2} \sim 1000$ GeV if $m_0 = 1000$ GeV and around $m_{1/2} \sim 1500$ GeV if $m_0 = 2000$ GeV⁴. In both cases there are portions of the funnel regions with $A_0 < 0$ that are also compatible with $m_h \sim 119$ GeV, as well as portions of the $\tilde{\tau}_1$ coannihilation strip with $A_0 < 0$ for $m_0 = 1000$ GeV and the $A > 0$ portion of the focus-point strip for $m_0 = 2000$ GeV, but $m_h = 125$ GeV is again nowhere to be seen.

4 WMAP Strips for $\tan\beta = 10, 40$ and 55

In light of the above illustrations, we will consider the detectability of neutralino dark matter along some characteristic WMAP strips in the CMSSM parameter space, paying particular attention to examples where $m_h \sim 119$ or 125 GeV.

We first consider examples with $\tan\beta = 10$. Comparing the left panel of Fig. 2 with the upper left panels of Figs. 3 and 4, and the left panel of Fig. 5, we see that the values of m_h along the $\tilde{\tau}_1 - \chi$ coannihilation strip increase only slowly with A_0/m_0 . Accordingly, in the following we consider this strip in the cases $A_0 = 0$ and $A_0 = 2.5m_0$. These are parametrized approximately by (here and in the following equations, dimensionful parame-

⁴These funnels have been coloured only in the range $\Omega_\chi h^2 = 0.112 \pm 0.012$ allowed by WMAP at the $2 - \sigma$ level.

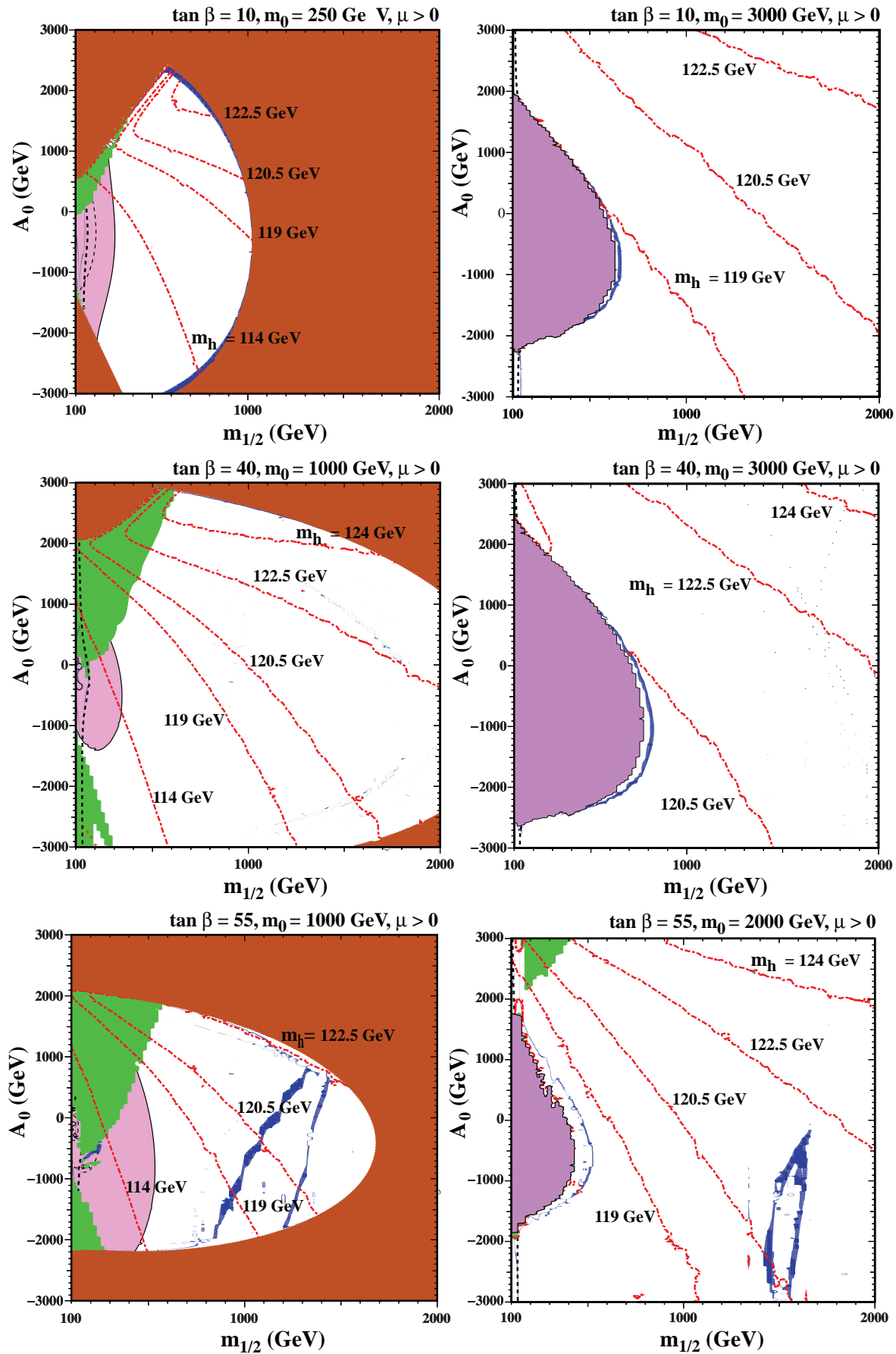


Figure 6: Representative $(m_{1/2}, A_0)$ planes for $\mu > 0$, $\tan \beta = 10$ with $m_0 = 250$ GeV (top left panel) and 3000 GeV (top right panel), or $\tan \beta = 40$ with $m_0 = 1000$ GeV (middle left panel) and 3000 GeV (middle right panel), and for $\tan \beta = 55$ with $m_0 = 1000$ GeV (bottom left panel) and 2000 GeV (bottom right panel), with the same shadings and contours as previously.

ters are expressed in GeV units):

$$m_0 = 0.24 m_{1/2} - 0.49, \quad A_0 = 0, \quad (1)$$

$$m_0 = 0.25 m_{1/2} + 3.50, \quad A_0 = 2.5m_0. \quad (2)$$

Values of $m_h \sim 119$ GeV are attained for relatively large values of $m_{1/2}$ along these strips. For comparison, we also discuss the focus-point strip for $\tan\beta = 10$ and $A_0 = 0$, which may be parametrized (a linear fit is inadequate in this case) by

$$m_0 = -0.0011 m_{1/2}^2 + 4.50 m_{1/2} + 750, \quad (3)$$

much of which is compatible with $m_h = 119$ GeV.

Several figures exhibit $\tilde{t}_1 - \chi$ coannihilation strips, which have not been much discussed in the dark matter detection literature, so we choose one example of this possibility. Specifically, the $\tilde{t}_1 - \chi$ strip in the left panel of Fig. 5 for $\tan\beta = 10$ and $A_0 = 2.5m_0$ is parametrized approximately by

$$m_0 = 2.40 m_{1/2} - 14. \quad (4)$$

Points all along this strip give values of m_h consistent with 119 GeV, taking into consideration the theoretical uncertainties in the calculation of m_h .

We also consider the corresponding $\tilde{\tau}_1 - \chi$ coannihilation strips for $\tan\beta = 40$, for $A_0 = 0$ and $2.5m_0$:

$$m_0 = 0.34 m_{1/2} + 82, \quad A_0 = 0, \quad (5)$$

$$m_0 = 0.75 m_{1/2} + 160, \quad A_0 = 2.5m_0. \quad (6)$$

We also consider some examples of strips with $\tan\beta = 55$. In the case $A_0 = 0$, shown in the right panel of Fig. 2, the $\tilde{\tau}_1 - \chi$ coannihilation strip morphs into the rapid H/A annihilation funnel when $m_{1/2} \sim 1000$ GeV, so we give parametrizations of both sides of the funnel:

$$\begin{aligned} m_0 &= 0.0010 m_{1/2}^2 - 0.49 m_{1/2} + 390, \\ m_0 &= 3.6 m_{1/2} - 3700. \end{aligned} \quad (7)$$

In this case, $m_h \sim 119$ GeV at relatively low values of $m_{1/2}$ below the funnel bifurcation, but values compatible with $m_h = 125$ GeV are not reached even at the tip of the funnel. As already commented, when $\tan\beta = 55$ we do not find generic solutions for $A_0 = 2.5m_0$, so we consider $A_0 = 2m_0$, as shown in the lower left panel of Fig. 4. This strip does not bifurcate into a funnel, and is parametrized by

$$m_0 = 1.9 m_{1/2} + 430. \quad (8)$$

In this case, values of $m_h \sim 125$ GeV and even larger are quite possible. Finally, we consider the focus-point strip for $\tan\beta = 55$ and $A_0 = 0$:

$$m_0 = -0.0011 m_{1/2}^2 + 3.8 m_{1/2} + 290, \quad (9)$$

where (we recall) all dimensionful parameters in the above equations are expressed in GeV units.

5 The Higgs Mass and Dark Matter Scattering along WMAP Strips

We now discuss the the spin-independent dark matter scattering cross section along the WMAP strips introduced in the previous Section, and correlate it with the predicted mass of the Higgs boson.

The left panel of Fig. 7 shows m_h (as calculated using `FeynHiggs`) along the WMAP $\tilde{\tau}_1 - \chi$ coannihilation strips parametrized by (1, 2) for $A_0 = 0$ (black line) and $A_0/m_0 = 2.5$ (red line), respectively. The upper ends of the stau coannihilation strips at $m_{1/2} \sim 900$ GeV are where $m_\chi = m_{\tilde{\tau}_1}$, and they are truncated by the LHC searches for missing-energy events at $m_{1/2} \sim 530$ GeV [31]. The portions of these and other strips allowed by the LHC missing-energy searches [31] are indicated by (purple) square brackets: [and the portions favoured by $g_\mu - 2$ are indicated by (pink) parentheses:). The absence of a) along a line indicates that no portion of the line is compatible with $g_\mu - 2$. We see that these constraints are incompatible for the $\tan\beta = 10$, $A_0 = 0$ strips shown.

As expected, increasing A_0 gives larger values of m_h , in this case by ~ 1 GeV, almost independently of $m_{1/2}$. We see that m_h is compatible with 119 GeV (within the estimated `FeynHiggs` error of ± 1.5 GeV, indicated by the lower green shaded horizontal band) for $m_{1/2} > 630$ GeV for $A_0 = 0$ and $m_{1/2} = 520$ GeV for $A_0/m_0 = 2.5$. Also shown in this panel as a blue line is m_h along the focus-point strip for $\tan\beta = 10$ and $A_0 = 0$ (3), which is cut off below $m_{1/2} \sim 300$ GeV by the LHC missing-energy searches [31], and is also compatible within errors with 119 GeV for $m_{1/2} > 370$ GeV. Finally, the green line shows m_h along the $\tilde{t}_1 - \chi$ coannihilation strip for $\tan\beta = 10$ and $A_0/m_0 = 2.5$, parametrized by (4)⁵. We see that m_h is somewhat higher along this line, and compatible within errors with $m_h = 119$ GeV for all the allowed range of $m_{1/2}$. On the other hand, none of these strips is compatible with $m_h = 125$ GeV (the upper green shaded horizontal band).

⁵We do not indicate LHC bounds here and in other cases in which the available results from LHC missing-energy searches [31] are insufficient to indicate which portions of this line might be excluded.

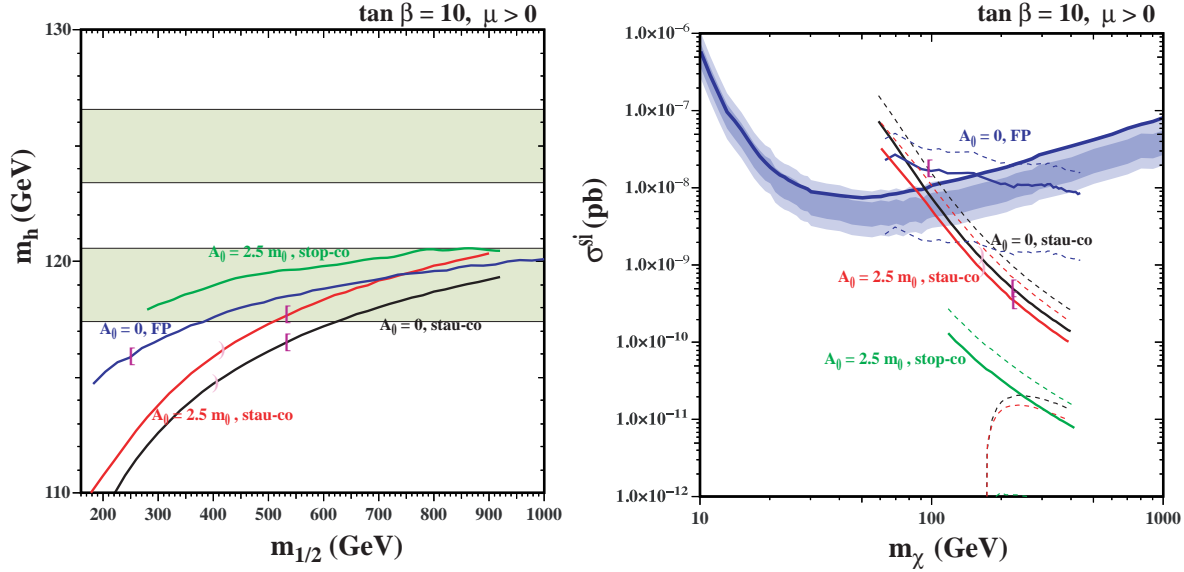


Figure 7: *Left panel: m_h as calculated using FeynHiggs (showing the band $m_h = 119 \pm 1.5$ GeV) and right panel: spin-independent elastic $\chi - p$ scattering cross section (showing the XENON100 upper limit [30] as a solid line accompanied by the shaded band described in the text), along the WMAP strips for $\tan \beta = 10$ - the $\tilde{\tau}_1 - \chi$ coannihilation strips for $A_0 = 0$ (1) (black) and $A_0/m_0 = 2.5$ (2) (red), the focus-point strip for $A_0 = 0$ (3) (blue), and the $\tilde{t}_1 - \chi$ coannihilation strip for $A_0/m_0 = 2.5$ (4) (green). In the left panels of this and subsequent figures, the ranges $m_h = 119 \pm 1.5$ GeV and 125 ± 1.5 GeV are green shaded horizontal bands. Here and subsequently, the portions of the WMAP strips allowed by the LHC missing-energy searches [31] are indicated by (purple) square brackets: [and the portions favoured by $g_\mu - 2$ are indicated by (pink) parentheses:).*

The right panel of Fig. 7 displays the spin-independent $\chi - p$ scattering cross section calculated along the same strips for $\tan \beta = 10$, displayed as functions of $m_\chi \sim 0.42 m_{1/2}$. The central values (shown as solid lines) are for $\Sigma_{\pi N} = 50$ MeV, and the dashed lines are for 64 and 36 MeV, respectively ⁶. These predictions are compared with the upper limit from the XENON100 experiment (solid dark blue line, the shaded bands are the ranges of the exclusion expected at the $\pm 1, 2\sigma$ levels) [30]. We see that the cross section along the $\tilde{\tau}_1 - \chi$ coannihilation strip for $A_0/m_0 = 2.5$ (shown in red) is somewhat lower than for $A_0 = 0$ (shown in black), though the difference is much less than the hadronic uncertainty in the cross section. If $\Sigma_{\pi N} = 50$ MeV, the portions $m_\chi < 80, 90$ GeV would be excluded by the XENON100 experiment [30], and the LHC missing-energy searches [31] and the hypothetical $m_h = 119$ GeV measurement would suggest a cross section $< 10^{-9}$ pb. The cross section along the focus-point strip (shown in blue) is significantly higher, particularly for large m_χ .

⁶See [20] for a discussion of the uncertainty in this parameter.

This reflects the fact that along this strip the relic density is brought into the WMAP range by $\chi - \chi$ annihilations alone, whereas coannihilation processes are important along the other strips. Thus, the $\chi - \chi$ annihilation cross section is higher along this strip, and the correspondingly also the elastic scattering cross section ⁷. The XENON100 experiment [30] imposes $m_\chi > 150$ GeV along this line, if $\Sigma_{\pi N} = 50$ MeV. The elastic scattering cross section is lowest of all along the $\tilde{t}_1 - \chi$ coannihilation strip (shown in green). This is because in this case the coannihilating partner particle is strongly-interacting, and the weights of $\tilde{t}_1 - \chi$ coannihilations and $\tilde{t}_1 - \tilde{t}_1$ and $\tilde{t}_1 - \tilde{t}_1$ annihilations are enhanced relative to the corresponding processes along the $\tilde{\tau}_1 - \chi$ coannihilation strip, so the role of $\chi - \chi$ annihilation is reduced, and similarly the elastic scattering cross section, which is far below the XENON100 upper limit.

The left panel of Fig. 8 displays the values of m_h along various WMAP strips for $\tan \beta = 40$. As before, the black line is for the $\tilde{\tau}_1 - \chi$ coannihilation strip with $A_0 = 0$ (5), and the (substantially higher) red line is for the corresponding strip with $A_0/m_0 = 2.5$ (6). In this case, the coannihilation strip for $A_0 = 0$ extends to $m_{1/2} \sim 1100$ GeV before terminating where $m_\chi = m_{\tilde{\tau}_1}$, whereas the strip for $A_0 = 2.5$ extends to $m_{1/2} \sim 1300$ GeV. The lower bounds on $m_{1/2}$ along these strips due to $b \rightarrow s\gamma$ are indicated by green brackets $\{$. The $A_0 = 0$ case is compatible with $m_h = 119$ GeV for $m_{1/2} > 550$ GeV (almost corresponding to the LHC missing-energy constraint [31]), and the $A_0/m_0 = 2.5$ case is compatible with $m_h = 125$ GeV for $m_{1/2} > 700$ GeV, within the `FeynHiggs` uncertainty of ± 1.5 GeV, as indicated by the horizontal bands. We see in the right panel of Fig. 8 that the elastic scattering cross section for $A_0/m_0 = 2.5$ (red) is smaller by almost an order of magnitude than that for $A_0 = 0$ (black), with the (optimistic) red dashed line for $A_0/m_0 = 2.5$ with $\Sigma_{\pi N} = 64$ MeV lying below the $\Sigma_{\pi N} = 50$ MeV value for $A_0 = 0$. Coupled with the lower limit $m_{1/2} > 700$ MeV required to be compatible with $m_h = 125$ GeV, we see that confirmation of this Higgs mass would suggest a cross section below 10^{-9} pb in this model. On the other hand, the XENON100 experiment [30] already requires $m_\chi > 150$ GeV if $A_0 = 0$ and $\Sigma_{\pi N} = 50$ MeV.

The left panel of Fig. 9 displays the values of m_h along various WMAP strips for $\tan \beta = 55$. As before, the black line is the $\tilde{\tau}_1 - \chi$ coannihilation for $A_0 = 0$ (7), and is actually doubled for $m_{1/2} > 1200$ GeV before terminating at $m_{1/2} \sim 1600$ GeV, corresponding to the two sides of the rapid-annihilation funnel, though the corresponding values of m_h are

⁷This connection is only qualitative, since the processes dominating t -channel exchange are not identical with the processes dominating s -channel annihilation, and the cosmological annihilations involve a mixture of P - and S -wave annihilations.

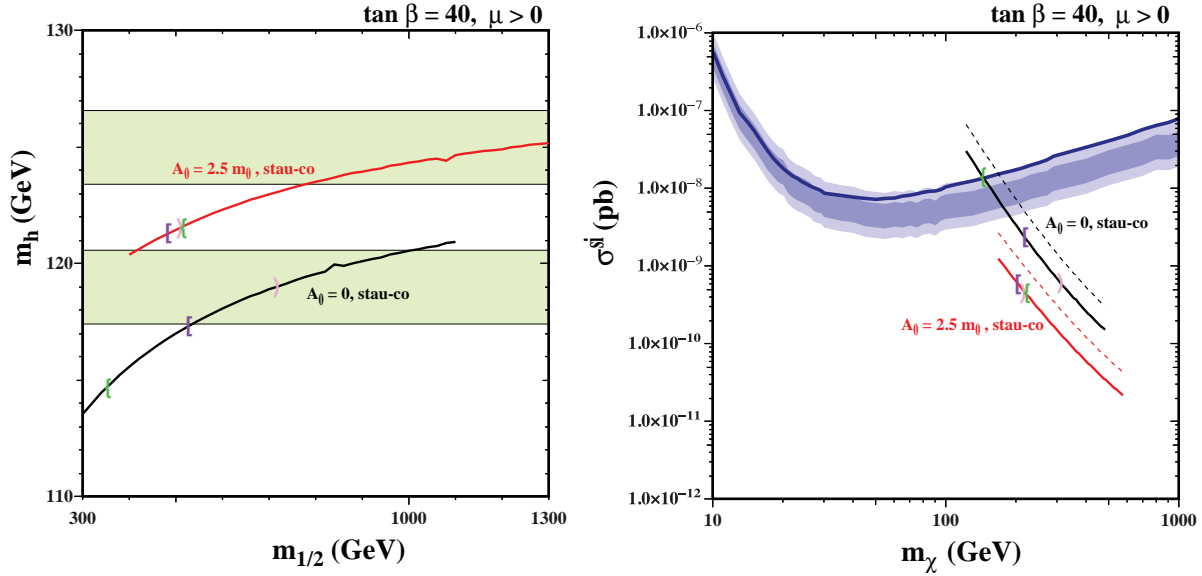


Figure 8: *Left panel: m_h as calculated using FeynHiggs (showing the bands $m_h = 119 \pm 1.5$ GeV and 125 ± 1.5 GeV) and right panel: spin-independent elastic $\chi - p$ scattering cross section (showing the XENON100 exclusion [30] as in Fig. 7), along WMAP strips for $\tan \beta = 40$ - the $\tilde{\tau}_1 - \chi$ coannihilation strips for $A_0 = 0$ (5) (black) and $A_0/m_0 = 2.5$ (red) (6). The lower bounds on $m_{1/2}$ along these strips due to $b \rightarrow s\gamma$ are indicated by green brackets { .*

very similar. In this case, we see that a range of $m_{1/2}$ is compatible with $g_\mu - 2$ as well as the LHC missing-energy searches and $m_h = 119$ GeV. The red line is for the $\tilde{\tau}_1 - \chi$ coannihilation strip with $A_0/m_0 = 2.0$ (8), as we do not find generic consistent solutions for $\tan \beta = 55$ and $A_0/m_0 = 2.5$. As in Fig. 7, the blue line is for the focus-point strip with $A_0 = 0$ (9). We see that $m_h = 119$ GeV is compatible with the $A_0 = 0$ coannihilation strip for $m_{1/2} > 600$ GeV, and with the $A_0 = 0$ focus-point strip for $m_{1/2} > 400$ GeV. However, only the $\tilde{\tau}_1 - \chi$ coannihilation strip with $A_0/m_0 = 2.0$ is compatible with $m_h = 125$ GeV, and this for all values of $m_{1/2}$.

The right panel of Fig. 9 displays the corresponding elastic scattering cross section along the same strips. As in Fig. 7, the focus-point strip yields the highest cross section, and as there and in Fig. 8, the cross section for $A_0 = 0$ is larger than that for $A_0/m_0 > 0$. This time, the cross section for $A_0/m_0 = 2.0$ is smaller than that for $A_0 = 0$ by more than an order of magnitude, and is again always $< 10^{-9}$ pb, even for the optimistic value $\Sigma_{\pi N} = 64$ MeV. Along the focus-point strip, on the other hand, the cross section could be as large as the XENON100 upper limit.

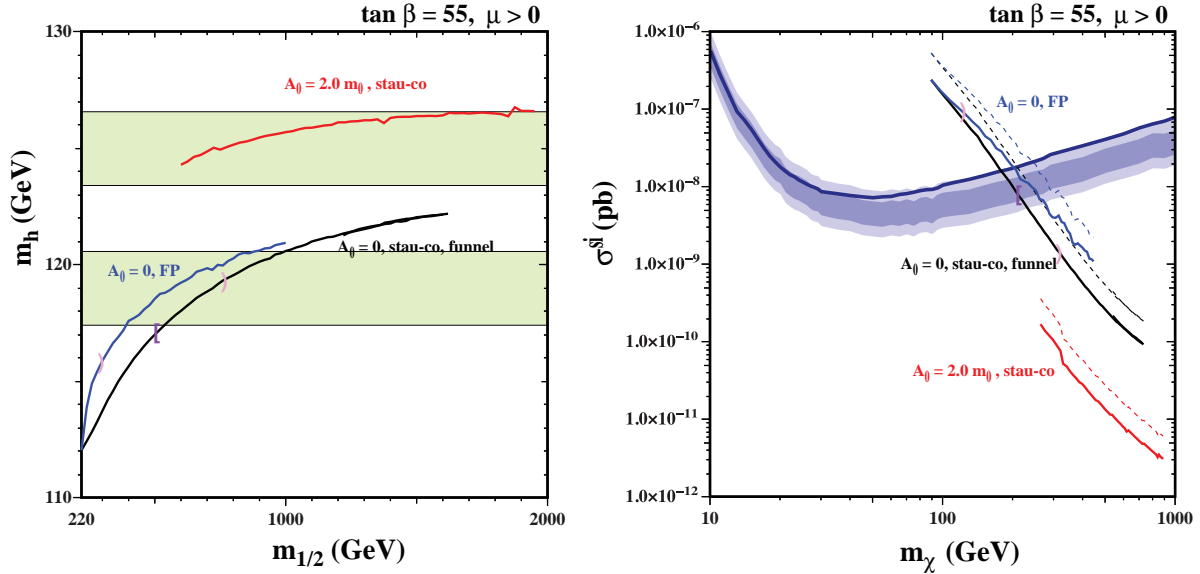


Figure 9: *Left panel: m_h as calculated using FeynHiggs (showing the bands $m_h = 119 \pm 1.5$ GeV and 125 ± 1.5 GeV) and right panel: spin-independent elastic $\chi - p$ scattering cross section (showing the XENON100 exclusion [30] as in Fig. 7), along WMAP strips for $\tan \beta = 55$ - the $\tilde{\tau}_1 - \chi$ coannihilation strips for $A_0 = 0$ (7) (black) and $A_0/m_0 = 2.0$ (8) (red), and the focus-point strip for $A_0 = 0$ (9) (green).*

6 Summary

We have discussed in this paper the interplay between a hypothetical measurement of the mass of the Higgs boson and spin-independent elastic dark matter scattering, in the context of WMAP strips in the $(m_{1/2}, m_0)$ planes of the CMSSM. In the past, it has been common to discuss planes with $A_0 = 0$ and various values of $\tan \beta \in [10, 55]$. However, previous studies [24, 27, 29] have shown that $A_0 > 0$ may be preferred, so we have explored this possibility in this paper. Among the examples we consider is a $\tilde{t}_1 - \chi$ coannihilation strip, a possibility that does not arise if $A_0 = 0$, and which has not been extensively studied in the dark matter detection literature.

Positive values of A_0 generally yield larger values of m_h than for $A_0 = 0$, which may be preferred in light of the LHC ‘hint’ that $m_h \sim 125$ GeV, though $m_h \sim 119$ GeV may still be a possibility. As could be anticipated from previous studies, only limited portions of the WMAP strips are compatible with $m_h \sim 125$ GeV, whereas larger portions are compatible with $m_h \sim 119$ GeV. In addition to $\tilde{\tau}_1 - \chi$ coannihilation strips with $\tan \beta \sim 40$ or more and $A_0 \sim 2m_0$ or more, which are reflected in Figs. 2 and 3 of [27], we also find that some portion of the $\tilde{\tau}_1 - \chi$ coannihilation strip for $\tan \beta = 10$ may also be compatible with $m_h \sim 125$ GeV within the FeynHiggs uncertainty of ± 1.5 GeV if A_0 is very large, e.g., $A_0 = 3000$ GeV,

$m_{1/2} \sim 900$ GeV and $m_0 \sim 350$ GeV. Such points would populate the low- $\tan\beta$ tail of the 68% CL region in the CMSSM ($\tan\beta, m_{1/2}$) plane shown in Fig. 3 of [27]. On the other hand, most supergravity models have $A_0 = c.m_0$ with $c \in [-3, 3]$, so this example might not arise in such scenarios.

CMSSM models lying along WMAP-compatible $\tilde{\tau}_1 - \chi$ coannihilation strips with $A_0/m_0 > 0$ generally have lower spin-independent elastic dark matter scattering cross sections than the corresponding cases with $A_0 = 0$. Some models with low m_χ and m_h are already excluded by the XENON100 upper limit on dark matter scattering, but models with $m_h \sim 125$ GeV generally yield cross sections well below this limit, typically $< 10^{-9}$ pb. It will be interesting to use some of the strips discussed here to benchmark other astrophysical dark matter strategies, e.g., indirect searches for $\chi - \chi$ annihilations that yield energetic neutrinos or photons. However, the general (loose) correlation between elastic scattering and relic annihilation suggests that the rates for such processes may also be suppressed in many models compatible with $m_h \sim 125$ GeV.

Acknowledgements

This work has been supported in part by the London Centre for Terauniverse Studies (LCTS), using funding from the European Research Council via the Advanced Investigator Grant 267352. The work of K.A.O. is also supported in part by DOE grant DE-FG02-94ER-40823 at the University of Minnesota.

References

- [1] M. Baak *et al.*, arXiv:1107.0975 [hep-ph].
- [2] J. R. Ellis, G. Ridolfi and F. Zwirner, Phys. Lett. B **257** (1991) 83; Phys. Lett. B **262** (1991) 477; Yasuhiro Okada, Masahiro Yamaguchi and Tsutomu Yanagida, Phys. Lett. B **262**, 54, 1991; Prog. Theor. Phys. **85** (1991) 1; A. Yamada, Phys. Lett. B **263** (1991) 233; Howard E. Haber and Ralf Hempfling, Phys. Rev. Lett. **66** (1991) 1815; M. Drees and M. M. Nojiri, Phys. Rev. D **45** (1992) 2482; P. H. Chankowski, S. Pokorski and J. Rosiek, Phys. Lett. B **274** (1992) 191; Phys. Lett. B **286** (1992) 307.
- [3] The most recent combination of ATLAS and CMS results may be found in: ATLAS and CMS Collaborations, <https://cdsweb.cern.ch/record/1399607/files/HIG-11-023-pas.pdf>.

- [4] ATLAS Collaboration, arXiv:1202.1408 [hep-ex]; arXiv:1202.1414 [hep-ex]; arXiv:1202.1415 [hep-ex]; arXiv:1202.1636 [hep-ex].
- [5] CMS Collaboration, arXiv:1202.1416 [hep-ex]; arXiv:1202.1487 [hep-ex]; arXiv:1202.1488 [hep-ex]; arXiv:1202.1489 [hep-ex]; arXiv:1202.1997 [hep-ex].
- [6] H. Goldberg, Phys. Rev. Lett. **50** (1983) 1419; J. Ellis, J. Hagelin, D. Nanopoulos, K. Olive and M. Srednicki, Nucl. Phys. B **238** (1984) 453.
- [7] M. Drees and M. M. Nojiri, Phys. Rev. D **47** (1993) 376 [arXiv:hep-ph/9207234]; H. Baer and M. Brhlik, Phys. Rev. D **53** (1996) 597 [arXiv:hep-ph/9508321]; Phys. Rev. D **57** (1998) 567 [arXiv:hep-ph/9706509]; H. Baer, M. Brhlik, M. A. Diaz, J. Ferrandis, P. Mercadante, P. Quintana and X. Tata, Phys. Rev. D **63** (2001) 015007 [arXiv:hep-ph/0005027].
- [8] G. L. Kane, C. F. Kolda, L. Roszkowski and J. D. Wells, Phys. Rev. D **49** (1994) 6173 [arXiv:hep-ph/9312272]; J. R. Ellis, T. Falk, K. A. Olive and M. Schmitt, Phys. Lett. B **388** (1996) 97 [arXiv:hep-ph/9607292]; Phys. Lett. B **413** (1997) 355 [arXiv:hep-ph/9705444]; J. R. Ellis, T. Falk, G. Ganis, K. A. Olive and M. Schmitt, Phys. Rev. D **58** (1998) 095002 [arXiv:hep-ph/9801445]; V. D. Barger and C. Kao, Phys. Rev. D **57** (1998) 3131 [arXiv:hep-ph/9704403]; J. R. Ellis, T. Falk, G. Ganis and K. A. Olive, Phys. Rev. D **62** (2000) 075010 [arXiv:hep-ph/0004169].
- [9] J. R. Ellis, T. Falk, G. Ganis, K. A. Olive and M. Srednicki, Phys. Lett. B **510** (2001) 236 [arXiv:hep-ph/0102098].
- [10] V. D. Barger and C. Kao, Phys. Lett. B **518** (2001) 117 [arXiv:hep-ph/0106189]; L. Roszkowski, R. Ruiz de Austri and T. Nihei, JHEP **0108** (2001) 024 [arXiv:hep-ph/0106334]; A. Djouadi, M. Drees and J. L. Kneur, JHEP **0108** (2001) 055 [arXiv:hep-ph/0107316]; U. Chattopadhyay, A. Corsetti and P. Nath, Phys. Rev. D **66** (2002) 035003 [arXiv:hep-ph/0201001]; J. R. Ellis, K. A. Olive and Y. Santoso, New Jour. Phys. **4** (2002) 32 [arXiv:hep-ph/0202110]; H. Baer, C. Balazs, A. Belyaev, J. K. Mizukoshi, X. Tata and Y. Wang, JHEP **0207** (2002) 050 [arXiv:hep-ph/0205325]; R. Arnowitt and B. Dutta, arXiv:hep-ph/0211417.
- [11] J. R. Ellis, K. A. Olive, Y. Santoso and V. C. Spanos, Phys. Lett. B **565** (2003) 176 [arXiv:hep-ph/0303043].

- [12] H. Baer and C. Balazs, JCAP **0305**, 006 (2003) [arXiv:hep-ph/0303114]; A. B. Lahanas and D. V. Nanopoulos, Phys. Lett. B **568**, 55 (2003) [arXiv:hep-ph/0303130]; U. Chattopadhyay, A. Corsetti and P. Nath, Phys. Rev. D **68**, 035005 (2003) [arXiv:hep-ph/0303201]; C. Munoz, Int. J. Mod. Phys. A **19**, 3093 (2004) [arXiv:hep-ph/0309346]; R. Arnowitt, B. Dutta and B. Hu, arXiv:hep-ph/0310103. J. Ellis and K. A. Olive, arXiv:1001.3651 [astro-ph.CO].
- [13] O. Buchmueller *et al.*, Phys. Lett. B **657** (2007) 87 [arXiv:0707.3447 [hep-ph]]; O. Buchmueller *et al.*, JHEP **0809** (2008) 117 [arXiv:0808.4128 [hep-ph]]; O. Buchmueller *et al.*, Eur. Phys. J. C **64** (2009) 391 [arXiv:0907.5568 [hep-ph]].
- [14] E. Komatsu *et al.* [WMAP Collaboration], Astrophys. J. Suppl. **192** (2011) 18 [arXiv:1001.4538 [astro-ph.CO]].
- [15] J. Ellis, T. Falk, and K.A. Olive, Phys. Lett. **B444** (1998) 367 [arXiv:hep-ph/9810360]; J. Ellis, T. Falk, K.A. Olive, and M. Srednicki, *Astr. Part. Phys.* **13** (2000) 181 [Erratum-ibid. **15** (2001) 413] [arXiv:hep-ph/9905481].
- [16] J. L. Feng, K. T. Matchev and T. Moroi, *Phys. Rev. D* **61** (2000) 075005 [arXiv:hep-ph/9909334].
- [17] C. Boehm, A. Djouadi and M. Drees, Phys. Rev. D **62** (2000) 035012 [arXiv:hep-ph/9911496]; J. R. Ellis, K. A. Olive and Y. Santoso, *Astropart. Phys.* **18** (2003) 395 [arXiv:hep-ph/0112113]; K. Huitu, L. Leinonen and J. Laamanen, Phys. Rev. D **84**, 075021 (2011) [arXiv:1107.2128 [hep-ph]].
- [18] M. Battaglia *et al.*, Eur. Phys. J. C **22**, 535 (2001) [arXiv:hep-ph/0106204]; M. Battaglia, A. De Roeck, J. R. Ellis, F. Gianotti, K. A. Olive and L. Pape, Eur. Phys. J. C **33**, 273 (2004) [arXiv:hep-ph/0306219]; E. A. Baltz, M. Battaglia, M. E. Peskin and T. Wizansky, Phys. Rev. D **74**, 103521 (2006) [hep-ph/0602187]; A. De Roeck, J. R. Ellis, F. Gianotti, F. Moortgat, K. A. Olive and L. Pape, Eur. Phys. J. C **49**, 1041 (2007) [hep-ph/0508198]; B. C. Allanach, M. Battaglia, G. A. Blair, M. S. Carena, A. De Roeck, A. Dedes, A. Djouadi and D. Gerdes *et al.*, Eur. Phys. J. C **25**, 113 (2002) [hep-ph/0202233]; J. A. Aguilar-Saavedra, A. Ali, B. C. Allanach, R. L. Arnowitt, H. A. Baer, J. A. Bagger, C. Balazs and V. D. Barger *et al.*, Eur. Phys. J. C **46**, 43 (2006) [hep-ph/0511344]; J. Ellis, T. Hahn, S. Heinemeyer, K. A. Olive and G. Weiglein, JHEP **0710**, 092 (2007) [arXiv:0709.0098 [hep-ph]].

- [19] J. R. Ellis, J. L. Feng, A. Ferstl, K. T. Matchev and K. A. Olive, Eur. Phys. J. C **24**, 311 (2002) [arXiv:astro-ph/0110225].
- [20] J. R. Ellis, K. A. Olive and C. Savage, Phys. Rev. D **77**, 065026 (2008) [arXiv:0801.3656 [hep-ph]].
- [21] J. Ellis, K. A. Olive, C. Savage and V. C. Spanos, Phys. Rev. D **81**, 085004 (2010) [arXiv:0912.3137 [hep-ph]].
- [22] J. Ellis, K. A. Olive and V. C. Spanos, JCAP **1110**, 024 (2011) [arXiv:1106.0768 [hep-ph]].
- [23] S. S. AbdusSalam, B. C. Allanach, H. K. Dreiner, J. Ellis, U. Ellwanger, J. Gunion, S. Heinemeyer and M. Kraemer *et al.*, Eur. Phys. J. C **71**, 1835 (2011) [arXiv:1109.3859 [hep-ph]].
- [24] J. R. Ellis, D. V. Nanopoulos, K. A. Olive and Y. Santoso, Phys. Lett. B **633**, 583 (2006) [arXiv:hep-ph/0509331].
- [25] O. Buchmueller *et al.*, Eur. Phys. J. C **71** (2011) 1634 [arXiv:1102.4585 [hep-ph]]; O. Buchmueller *et al.*, Eur. Phys. J. C **71** (2011) 1722 [arXiv:1106.2529 [hep-ph]].
- [26] O. Buchmueller, R. Cavanaugh, A. De Roeck, M. J. Dolan, J. R. Ellis, H. Flacher, S. Heinemeyer and G. Isidori *et al.*, arXiv:1110.3568 [hep-ph].
- [27] O. Buchmueller, R. Cavanaugh, A. De Roeck, M. J. Dolan, J. R. Ellis, H. Flacher, S. Heinemeyer and G. Isidori *et al.*, arXiv:1112.3564 [hep-ph].
- [28] G. Degrassi, S. Heinemeyer, W. Hollik, P. Slavich and G. Weiglein, Eur. Phys. J. C **28** (2003) 133 [arXiv:hep-ph/0212020]; S. Heinemeyer, W. Hollik and G. Weiglein, Eur. Phys. J. C **9** (1999) 343 [arXiv:hep-ph/9812472]; S. Heinemeyer, W. Hollik and G. Weiglein, Comput. Phys. Commun. **124** (2000) 76 [arXiv:hep-ph/9812320]; M. Frank *et al.*, JHEP **0702** (2007) 047 [arXiv:hep-ph/0611326]; See <http://www.feynhiggs.de> .
- [29] H. Baer, V. Barger and A. Mustafayev, arXiv:1112.3017 [hep-ph]; J. L. Feng, K. T. Matchev and D. Sanford, arXiv:1112.3021 [hep-ph]; S. Heinemeyer, O. Stal and G. Weiglein, arXiv:1112.3026 [hep-ph]; A. Arbey, M. Battaglia, A. Djouadi, F. Mahmoudi and J. Quevillon, arXiv:1112.3028 [hep-ph]; P. Draper, P. Meade, M. Reece and D. Shih, arXiv:1112.3068 [hep-ph]; S. Akula, B. Altunkaynak, D. Feldman, P. Nath and G. Peim, arXiv:1112.3645 [hep-ph]; M. Kadastik, K. Kannike, A. Racioppi and

- M. Raidal, arXiv:1112.3647 [hep-ph]; C. Strege, G. Bertone, D. G. Cerdeno, M. Fornasa, R. R. de Austri and R. Trotta, arXiv:1112.4192 [hep-ph]; N. Karagiannakis, G. Lazarides and C. Pallis, arXiv:1201.2111 [hep-ph]; L. Aparicio, D. G. Cerdeno and L. E. Ibanez, arXiv:1202.0822 [hep-ph].
- [30] E. Aprile *et al.* [XENON100 Collaboration], *Phys. Rev. Lett.* **107** (2011) 131302 [arXiv:1104.2549 [astro-ph.CO]].
- [31] S. Chatrchyan *et al.* [CMS Collaboration], *Phys. Rev. Lett.* **107**, 221804 (2011) [arXiv:1109.2352 [hep-ex]]; G. Aad *et al.* [ATLAS Collaboration], arXiv:1109.6572 [hep-ex].
- [32] M. Misiak *et al.*, *Phys. Rev. Lett.* **98** (2007) 022002 [arXiv:hep-ph/0609232]; M. Ciuchini, G. Degrossi, P. Gambino and G. F. Giudice, *Nucl. Phys. B* **534** (1998) 3 [arXiv:hep-ph/9806308]; G. Degrossi, P. Gambino and G. F. Giudice, *JHEP* **0012** (2000) 009 [arXiv:hep-ph/0009337]; M. S. Carena, D. Garcia, U. Nierste and C. E. M. Wagner, *Phys. Lett. B* **499** (2001) 141 [arXiv:hep-ph/0010003]; G. D'Ambrosio, G. F. Giudice, G. Isidori and A. Strumia, *Nucl. Phys. B* **645** (2002) 155 [arXiv:hep-ph/0207036]; The Heavy Flavor Averaging Group, D. Asner *et al.*, arXiv:1010.1589 [hep-ex], with updates available at http://www.slac.stanford.edu/xorg/hfag/osc/end_2009.
- [33] G. Bennett *et al.* [The Muon g-2 Collaboration], *Phys. Rev. Lett.* **92** (2004) 161802, [arXiv:hep-ex/0401008]; and *Phys. Rev. D* **73** (2006) 072003 [arXiv:hep-ex/0602035].
- [34] CDF and D0 Collaborations, arXiv:1007.3178 [hep-ex].
- [35] Information about this code is available from K. A. Olive: it contains important contributions from T. Falk, A. Ferstl, G. Ganis, A. Mustafayev, J. McDonald, K. A. Olive, P. Sandick, Y. Santoso and M. Srednicki.